

Variation of carrier density in semimetals via short-range correlation: a case study with nickelate NdNiO_2

Ruoshi Jiang (姜若诗),¹ Zi-Jian Lang (郎子健),¹ Tom Berlijn,² and Wei Ku (顧威)^{1,3,*}

¹*Tsung-Dao Lee Institute & School of Physics and Astronomy,
Shanghai Jiao Tong University, Shanghai 200240, China*

²*Center for Nanophase Materials Sciences, Oak Ridge National Laboratory, Oak Ridge, TN 37831, USA*

³*Key Laboratory of Artificial Structures and Quantum Control (Ministry of Education), Shanghai 200240, China*

(Dated: July 19, 2022)

Carrier density is one of the key controlling factors of material properties, particularly in controlling the essential correlations in strongly correlated materials. Typically, carrier density is externally tuned by doping or gating, and remains fixed below room temperature. Strangely, the carrier density in correlated semimetals is often found to vary sensitively to the external controls of small energy scale, such as temperature, magnetic field, and pressure. Here using the recently discovered nickelate superconductor as an example, we demonstrate a rather generic low-energy mechanism that short-range (non-collinear magnetic) correlation can reversely modulate the carrier density as well. Such a mutual influence between correlation and carrier density provides an extra ingredient for bifurcation of emergent phenomena. This special feature of correlated semimetals explains their versatile carrier density at low energy, and opens up new possibilities of functionalizing these materials.

The effect of electronic correlation on physical properties of strongly correlated materials is one of the most important topics in condensed matter physics. Unlike the kinetic energy which dominates the low-energy physics of weak interacting systems, correlation between electrons in strongly correlated materials can introduce significant complexity, leading to emergence of numerous phenomena, such as the interaction-driven metal-insulator transition [1, 2], colossal magnetoresistivity [3], unconventional superconductivity [4, 5], strange metallicity [6], bad metal behavior [7], and quantum spin liquid realization [8], etc. Naturally, the most essential quests of the field are centered around exploring these complex correlation effects and efficient means of their control for practical applications.

Among the key controlling factors of electronic correlation, carrier density is known to be the most effective. This naturally follows the fact that correlation results from influence of electrons onto each other and is therefore sensitive to their average distance, or their density. Indeed, one typically finds a rich diagram of phases in correlated materials hosting dramatically different behaviors upon tuning the carrier density in these materials [9, 10]. Well-known examples include cuprates [11], iron pnictides [12], manganites [13], titanates [14], ruthenates [15], cobaltates [16], twisted bilayer graphene [17, 18], all testifying the extreme efficiency of carrier density in tuning the correlation and in turns the physical properties.

In correlated semimetals, this strong sensitivity to density grants extra complexity and functionality due to semimetals' additional flexibility in carrier density. Unlike regular metals and insulators that have rather robust densities fixed by their chemical potentials, semimetals have the additional freedom in varying the carrier density since the chemical potential only pins the *difference* between the coexisting electron and hole carriers, not their sum. Indeed, for example in unconventional high-temperature superconductors such as FeSe [19] and nickelates [20], the observed strong temperature depen-

dent Hall coefficients suggests a sensitively varying carrier density. Such variation of carrier density is in good consistency with the apparent change of size of the Fermi surface observed in FeSe [21] by angular-resolved photoemission spectroscopy. As another example, in unconventional WTe_2 superconductor the Hall coefficient [22] displays a strong pressure dependence, and the carrier density changes balance over temperature as well [23]. These examples demonstrate the intimate connection between the rich physical behaviors and the versatile carrier density in correlated semimetal.

Therefore, two essential generic questions concerning the carrier density in correlated semimetals are 1) what key factors control the carrier density variation in these systems, and 2) how the carrier density is able to vary so efficiently against change of “weak” external conditions, for example temperature, pressure, or magnetic field. The strongest correlation due to strong intra-atomic repulsion is known to be able to enhance the effective mass of carriers [24–27] (which can potentially modify the carrier density in semimetals). However, the large energy scale of the local repulsion dictates that such mass enhancement is rather robust and thus unable to vary sensitively by “weak” (or low-energy) external conditions. Apparently, one needs to seek the answer in the physics of a much lower energy scale.

Here, based on realistic many-body Hamiltonian extracted from density functional theory (DFT) calculation [28, 29] of NdNiO_2 , we simulate how non-local magnetic correlation affects the carriers' one-body propagator. This is done by averaging over results of self-consistent Hartree-Fock calculations under various constrained *unordered* and *non-collinear* magnetic configurations. We find a clear systematic trend that scattering against stronger non-local anti-ferromagnetic correlation can damage more noticeably the kinetic energy of the hole carriers, leading to a more enhanced effective mass and in turn a smaller carrier density. Since non-local correlations, particularly those beyond the nearest neighbors, are typically of an order of a few tenth meV, they are generally the natural

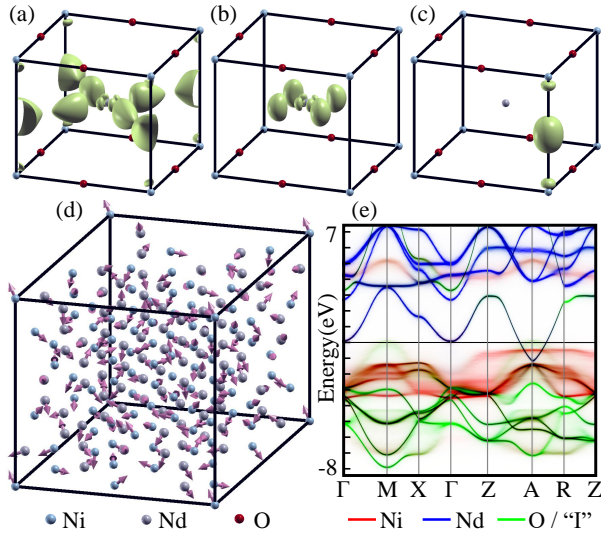


FIG. 1. (color online) Illustration of the Bloch orbital corresponding to the electron pocket at momentum (π, π, π) (a), showing a significant contribution in the interstitial region. A more complete basis thus should include an interstitial “I”-orbital (c) in addition to the Nd- d_{xy} Wannier orbital (b). (d) Illustration of *unordered non-collinear* magnetic configurations with spin directions of each magnetic atom denoted by the arrows. (e) An example of ensemble-averaged one-body spectral functions $A(k, m, \omega)$ corresponding to fully Curie-paramagnetic systems with no short-range correlation. Contributions from different orbitals, including the interstitial “I”-orbital are represented by different colors.

candidates to produce the observed carrier density variation in most correlated semimetals under the influence of weak external conditions. Finally, given that carrier density itself is a key controlling parameter for the strength of correlation, the latter’s effect on the former as reported here would create a nonlinear feedback. Such non-linearity is expected to enhance the system’s tendency toward bifurcating behaviors at lower energy, including for example a strongly correlated low-density state and a weakly correlated high-density one, thus enabling richer physics and more complex functionality of correlated semimetals.

Since our goal is to demonstrate the generic physical effect in real correlated semimetals, we proceed with the following simulation. First, we extract a realistic SU(2)-symmetric high-energy many-body Hamiltonian for the prototypical parent compound of the nickelate superconductor, NdNiO_2 from DFT calculations. Second, we compute the electronic one-body spectral function under randomly chosen *unordered* magnetic configurations that contains various constrained *non-collinear* spin directions with *negligibly small* long-range order parameters. Finally, we analyze the systematic trend of short-range correlation effects on the dressed band structure by averaging results from magnetic configurations of similar correlation strength.

Specifically, it is necessary for us to obtain a fully SU(2)-symmetric many-body interacting Hamiltonian, so that it is applicable to the various non-collinear magnetic fluctuation in real materials. We therefore demand that it must be able

to *simultaneously* reproduce the band structures from DFT calculations under various magnetic structures, including the fully ferromagnetic and fully anti-ferromagnetic ones. Furthermore, since this compound contains open-shelled (partially occupied) Nd f -orbitals and Ni d -orbitals, approximations like the “LDA+ U ” [30–32] or hybrid functionals [33] are necessary in the DFT calculations in order to ensure a realistic density. (Otherwise, these orbitals can collapse near the chemical potential and ruin the density profile of the system.) To this end, we apply the (LDA+ U)+(many-body) procedure [34, 35] to extract the realistic many-body Hamiltonian. (See Supplementary [32] for all technical details.)

Note that in disordered systems the orbital hybridization can vary strongly. It is therefore necessary to construct a more complete set of atomic-like Ni d -, O p - and Nd d -Wannier orbitals [34–39] without down-folding to a smaller low-energy subspace. In addition, the Bloch orbital corresponding to the electron pocket at momentum (π, π, π) shown in Fig. 1 (a) contains a significant contribution in the empty space above Ni atoms [40]. It is thus highly beneficial to include an additional interstitial “I”-orbital [c.f. Fig. 1(c)]. This more complete basis would contain symmetry-respecting Wannier orbitals that are almost atomically local in space and nearly configuration independent. This would greatly facilitate the ensemble average that follows since results from different configurations are represented in nearly identical basis set.

The resulting SU(2)-symmetric effective Hamiltonian reads:

$$H^{\text{eff}} = \sum_{i,m,v} \epsilon_m c_{imv}^\dagger c_{imv} + \sum_{i,i',m,m',v} t_{ii'mm'} c_{imv}^\dagger c_{i'm'v} \\ + \frac{1}{2} \sum_{i,m,m',m'',v,v'} U_{mm'm'm'} c_{imv}^\dagger c_{im''v'} c_{im''v'} c_{im'v} \\ - \frac{1}{2} \sum_{im,v,v'} J_m \mathbf{S}_i^f \cdot c_{imv}^\dagger \mathbf{\sigma}_{vv'} c_{imv'}, \quad (1)$$

including one-body orbital energy ϵ and hopping strength t , and intra-atomic two-body interaction U among the Ni d -orbitals denoted by creation c_{imv}^\dagger and annihilation c_{imv} operators of orbitals m and spin v within unit cell i . (See Supplementary S3 [32] for the leading parameters.) Note that owing to the very large intra-atomic Coulomb repulsion among the Nd f -orbitals, their charge fluctuation can be safely integrated out, leaving only their $\frac{3}{2}$ -spin \mathbf{S}_i^f degrees of freedom and their ferromagnetic coupling J to the Nd d -orbitals in Eq. 1. Here σ denotes the usual vector of Pauli matrices.

Next, to simulate the impact of short-range correlation on the one-body propagator *in the absence* of long-range order, we construct many randomly oriented supercells of various shapes containing non-collinear magnetic configurations of Ni d -orbitals [c.f. Fig. 1(d)] and demand that the average order parameters (ferromagnetic or anti-ferromagnetic) be negligibly small. (See Supplementary S4 [32] for details.) (Since the Nd-Nd and Nd-Ni magnetic couplings are negligibly small, the directions of Nd spins are treated as completely random in our simulation.) Obviously, the size of the supercells must be

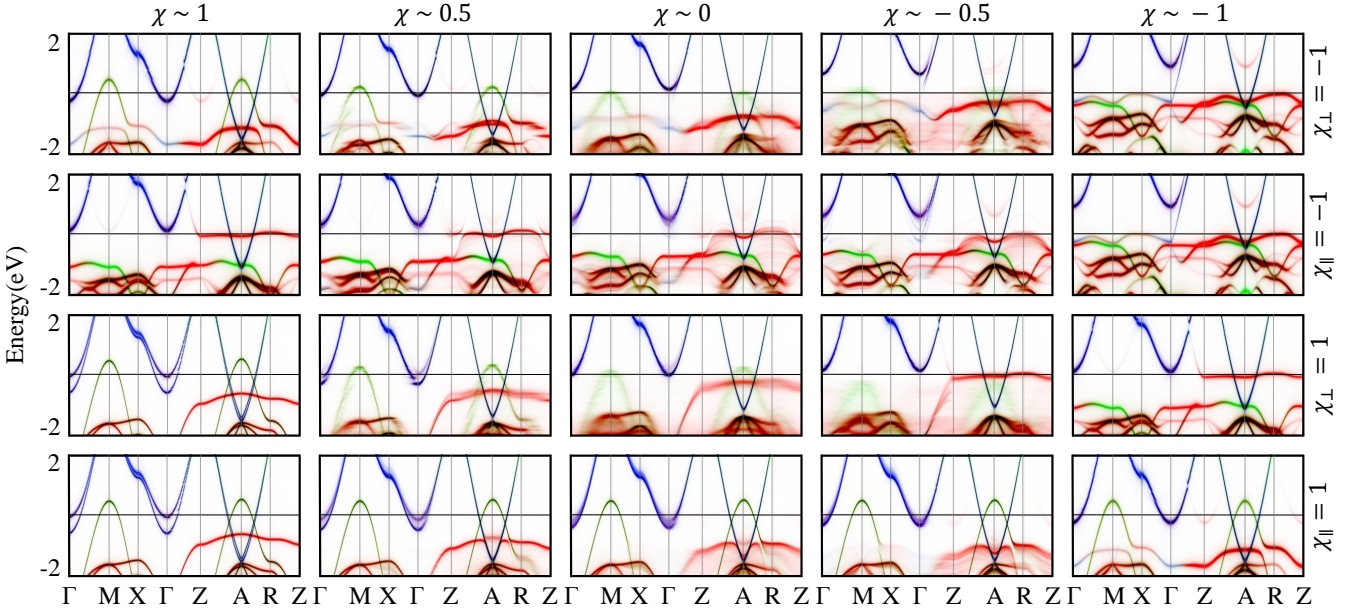


FIG. 2. (color online) Ensemble-averaged one-body spectral functions $A(k, m, \omega)$ under various nearest neighboring *non-collinear* intra-layer correlation χ_{\parallel} and inter-layer correlation χ_{\perp} , while keeping the other direction fixed as anti-ferromagnetic (top two rows) or ferromagnetic (bottom two rows). The color scheme is the same as in Fig. 1.

sufficiently large in such simulations to allow configurations with strong short-range correlation and yet negligible long-range order at the same time. Such a large supercell thus limits our options of affordable many-body methods, particularly considering the need for additional constraint on the spin directions in each magnetic configuration.

We therefore employ the self-consistent Hartree-Fock approximation to compute the frequency ω -dependent, orbital M -projected one-body spectral function,

$$A(K, M, \omega) = \sum_J |\langle KM | KJ \rangle|^2 \delta(\omega - \epsilon_{KJ}), \quad (2)$$

using the eigenvalue ϵ_{KJ} and eigenvector $|KJ\rangle$ corresponding to band J and crystal momentum K of each supercell, with spin directions constrained according to the magnetic configuration. The use of Hartree-Fock approximation makes the computation possible even for the large system size necessary for our investigation. It also offers a simple route to constrain the spin direction of each Ni atom of the magnetic configuration, by simply enforcing the one-body density matrix to be spin-diagonal along the specified spin direction in every self-consistent cycle.

We then categorize the configurations based on the strength of their nearest neighboring magnetic correlation between Ni $\frac{1}{2}$ -spins \mathbf{S}_i ,

$$\chi = \sum_{\langle i, i' \rangle} \mathbf{S}_i \cdot \mathbf{S}_{i'}, \quad (3)$$

and average the one-body spectral functions within each category. This average can be easily performed in the configuration-independent orbital basis (momentum k and orbital m) of the chemical formula unit, $A(k, m, \omega) =$

$\sum_{K, M} |\langle km | KM \rangle|^2 A(K, M, \omega)$, through the unfolding procedure [41], which also facilitates an easier visualization in the standard Brillouin zone. The chemical potential is then determined from the *averaged* one-body spectral function based on the total occupation of these orbitals.

Fig. 1(e) gives an example of the resulting ensemble-averaged unfolded one-body spectral function that corresponds to fully Curie-paramagnetic systems without short-range correlation $\chi \sim 0$ (as in the high temperature limit.) Notice that it displays many interesting characteristics distinct from results of typical non-magnetic calculations. For example, one observes significant smearing in some of the bands with Ni d -orbitals (in red), reflecting a shorter mean-free path and lifetime of quasi-particles corresponding to these bands. This is evidently from strong scattering against the unordered Ni $\frac{1}{2}$ -spins, since particles in the Ni d -shell would experience a strong spin-dependent self-energy that varies by a large scale of $U \sim 7$ eV in Eq. 1. In comparison, the scattering of Nd d -orbitals (in blue) against the Nd $f \frac{3}{2}$ -spins is obviously much less effective due to the rather small f - d spin coupling $J \sim 0.3$ eV in Eq. 1.

Concerning the influence of short-range magnetic correlation on the one-body spectral function, Fig. 2 summarizes our main result. The first row shows a clear trend that the size of the hole pocket around the $M = (\pi, \pi, 0)$ momentum reduces significantly, as the intra-layer magnetic correlation of the Ni-O layer changes from strongly ferromagnetic (left) to strongly anti-ferromagnetic (right) under a fixed anti-ferromagnetic inter-layer correlation χ_{\perp} . Correspondingly, the electron pockets around the $A = (\pi, \pi, \pi)$ momentum also shrink their size. A similar strong reduction of the Fermi pocket is also observed in the second row, when the inter-layer correlation

changes from ferromagnetic to anti-ferromagnetic while keeping the intra-layer correlation χ_{\parallel} anti-ferromagnetic. One therefore concludes that anti-ferromagnetic correlation can effectively reduce the Fermi pocket, or more essentially the carrier density.

This effect of correlation modulated carrier density in correlated semimetals can be more clearly demonstrated with Fig. 3(a), which quantifies the ensemble-averaged density of the electron carriers (and equivalently that of the hole carriers) corresponding to the first row in Fig. 2,

$$n_e = \left\langle \frac{1}{V} \int d^3K \sum_{J \in \{J_e\}} n_F(\epsilon_{KJ} - \mu) \right\rangle, \quad (4)$$

in which the summation involves only those bands corresponding to the electron pockets $\{J_e\}$, namely those with orbital character M predominantly from Nd and the interstitial ‘‘I’’, $\sum_{M \in \{Nd,I\}} |\langle KM|KJ \rangle|^2 > \frac{1}{2}$. Here V denotes the volume of the system with periodic boundary condition for each configuration, n_F the standard Fermi-Dirac distribution function, and μ the chemical potential obtained from the *ensemble averaged* one-body spectral function. (One can also estimate this density by measuring approximately the volume of the electron pockets, as long as the smearing of the band is not too severe.) Figure 3(a) demonstrates clearly that as the system develops stronger anti-ferromagnetic correlation in all directions, the carrier density can be very effectively suppressed in correlated semimetals. In this particular example, the suppression of carrier density can be more than *an order of magnitude*.

This short-range correlation-induced scattering offers a natural explanation to the key questions mentioned above in correlated semimetals. It not only produces a strong modulation of carrier density, but more importantly, this mechanism is active with a lower energy scale relevant to the experimental parameters. Specifically, unlike the above eV scale intra-atomic correlations, inter-atomic correlations in spin, orbital, or lattice channels are typically lower than 100 meV scale. It therefore responds more sensitively to external parameters, for example pressure, external field, disorder, doping, or temperature. Such a lower-energy tunability naturally makes these correlated semimetals ideal for real electronic devices.

It is important to emphasize that the effect observed here is from the short-range correlation, instead of the long-range order. Since a long-range order necessarily implies considerable short-range correlation, typical studies incorporating long-range order unavoidably inherit the impacts of short-range correlation as well. However, a system with strong short-range correlation does not necessarily host a long-range order when long-range fluctuation is present, for example due to itinerant carriers [42] or in lower dimension. It is therefore essential to distinguish cleanly the different physical roles of long-range order and short-range correlation. In our simulation, since the long-range order is intentionally turned off, our results make clear that it is really the short-range correlation, *not* the long-range order, that gives rise to the observed den-

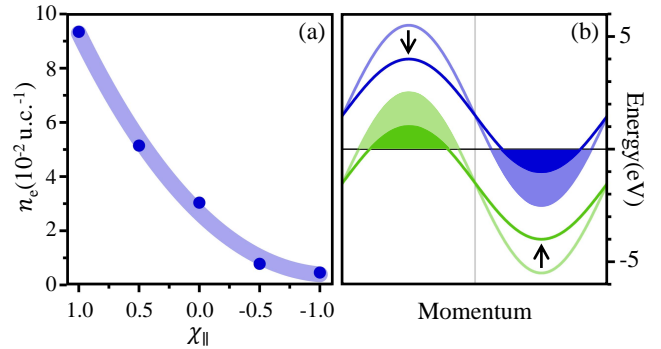


FIG. 3. (color online) (a) Significant suppression of carrier density under stronger intra-layer anti-ferromagnetic *non-collinear* correlation χ_{\parallel} , corresponding to the first row in Fig. 2. (b) Illustration of reduced carrier density via weakening of kinetic energy, showing smaller (green) electron- and (blue) hole-pockets.

sity modulation.

This essential effect of short-range correlation actually has an intuitive microscopic origin, namely the reduction of effective kinetic energy. As discussed above, due to the Pauli principle and the strong Hund’s coupling, when moving between neighboring Ni atoms, carriers encounter different degree of scattering probability: weaker with a nearly uniform (ferromagnetic) spin environment and stronger with rapidly varying spin orientation. Such a short-range spin-correlation dependent scattering would naturally reduces the effective kinetic energy of the low-energy carriers (via a non-local self-energy), independent of the absence or presence of long-range order. At longer length scale, this scattering would therefore lead to a reduction of the carrier bandwidth. As illustrated by the sketch in Fig. 3(b), this in turn shrinks the size of electron and hole Fermi pockets, and in other words reduces the carrier density.

The first and third rows of Fig. 2 confirm this intuitive picture. When the intra-layer spin orientation is more uniform ($\chi \sim 1$ ferromagnetic) the hole pocket around the M point is a hybrid of Ni *d*- and O *p*-orbital (in a green and red mixture). In great contrast, under stronger scattering against short-range anti-ferromagnetic correlation ($\chi \rightarrow -1$) the same becomes completely O *p*-orbital (in green) dominant, and the Ni orbital weight retracts from the Fermi level toward its orbital energy around -3 eV. This reflects exactly the above mechanism of kinetic energy reduction involving the Ni *d*-orbitals. (This tendency further strengthens the previous claim [43, 44] that hole carriers in this system are predominantly Zhang-Rice singlets containing important O *p*-orbital contributions.) On the hand, the forth row verifies the opposite situation that for such a quasi-2D layered materials as long as the intra-layer correlation is uniform or ferromagnetic, the damage of the intra-layer kinetic energy due to increasing inter-layer correlation is not significant, as expected from the above mechanism.

Note that even though our demonstration above focuses on carrier scattering due to magnetic correlation, the microscopic mechanism discussed here is generally applicable to all strong non-local correlation. Since all short-range charge- lattice-, or

orbital-correlations act to restrict the carrier motion to some degree regardless their origin, they produce similar effect of carrier density modulation in correlated semimetals.

From a general perspective, such a correlation modulation of carrier density in correlated semimetals opens up an interesting possibility of bifurcating behavior, toward either a weakly correlated metal or a strongly correlated system with much lower carrier density. Imagine engineering a correlated semimetal with high carrier density that hosts rather weak correlation. Upon enhancing the short-range correlation via a slight tuning of external parameter (for example temperature, pressure, chemical doping or even magnetic field), the induced suppression of kinetic energy would lead to a smaller carrier density. This in turn allows a stronger correlation, giving rise to a cascading effect toward a strongly correlated system with low carrier density. In the context of metal-insulator transition, such a bifurcation behavior might further promote Mott's proposal [2] of a first-order quantum phase transition.

Such tendency of bifurcation offers a simple explanation to the dramatic change of physical properties observed in many experiments. For example in Ni-based and Fe-based unconventional superconductors (both strongly correlated semimetals), Hall coefficient displays a strong temperature dependence [20, 45]. In standard interpretation, the data indicates a reduction of carrier density by more than an order of magnitude at low temperature. With the above bifurcating tendency, this unusual behavior is understandable. Similarly, the extreme sensitivity of superconductivity to the substrates and lattice constants in these materials [46, 47] may also be affected by such bifurcating tendency. Naturally, this mechanism suggests many possible routes of engineering functional semimetals that responds sensitively to the weak change of external conditions.

In summary, we identify a generic low-energy mechanism for the puzzling tunability of carrier density in correlated semimetals. Using recently discovered Ni-based unconventional superconductors as an example, we demonstrate that scattering against short-range (non-collinear spin) correlation can lead to a suppression of carrier density in correlated semimetals *regardless* whether a long-range order occurs. This can be understood microscopically as a consequence of suppressed average kinetic energy with semi-metals' unique flexibility of compensating electron- and hole-carrier density. This mechanism suggests an enhanced tendency toward bifurcating physical properties at low energy scale relevant to slight modulation of external parameters such as temperature or external field. Our proposal not only provides a natural and intuitive explanation for the observed exotic tunability of carrier density in many correlated semimetals, but also suggests routes to functionalize correlated semimetals for richer physical properties and wider scope of application in electronic devices.

This work is supported by National Natural Science Foundation of China (NSFC) No.11674220 and No.11745006 and Ministry of Science and Technology No.2016YFA0300500 and No.2016YFA0300501. A portion of this work was con-

ducted at the Center for Nanophase Materials Sciences, which is a DOE Office of Science User Facility.

SUPPLEMENTARY

1.Computational details of density functional calculation

For this prototypical case, we obtain the most relevant Hilbert space within ± 10 eV around the Fermi energy from the spin polarized LDA+ U [30, 31] electronic structure of the parent compound NdNiO₂, using the linearized augmented plane wave [48] implementation [49] of the density functional theory (DFT) [28, 29]. We take from Ref. [20] the lattice structure with lattice constant $a = b = 3.92\text{\AA}$, $c = 3.37\text{\AA}$, and the space group $P4/mmm$. We set $U - J = 0.6 - 0.06$ Ry = 7.344 eV for Ni d -orbitals, 0.20 – 0.00 Ry = 2.72 eV, 0.60 – 0.00 Ry = 8.16 eV for Nd d -, f -orbitals separately.

2.Extraction of many-body Hamiltonian

We aim at obtaining a realistic SU(2)-symmetric many-body Hamiltonian H^{eff} in Eq.(1). To ensure a DFT-like level of accuracy, we further demand that when under a similar approximation, our many-body Hamiltonian needs to reproduce the self-consistent DFT Hamiltonian (equivalently the electronic band structure). Since in LDA+ U the strong local electron-electron interaction is approximated in an effective Hartree-Fock manner [50], a proper connection can be naturally made on the Wannier states basis by matching the self-consistent Hartree-Fock solution of our SU(2)-symmetric H^{eff} with the self-consistent $H^{\text{LDA+}U}$ [35]. The requirement that the Hartree-Fock approximation of H^{eff} needs to reproduce the LDA+ U band structure within the subspace of the active orbitals results in a rather unique set of parameters in H^{eff} [35].

Specifically, since we demand that the self-consistent Hartree-Fock solution reproduce the self-consistent solution of the LDA+ U solution, the corresponding density matrix $\rho_{ivv'}$ must be identical in both cases when represented in the same set of Wannier orbitals. One can thus take $\rho_{ivv'}$ directly from the self-consistent LDA+ U solution in the Wannier basis. Furthermore, if one assumes that the structure of $U_{mm''m'''m'}$ follows the Slater integral [31, 51], the entire $U_{mm''m'''m'}$ can be fixed by just two parameters U_{eff} and J_{eff} . Combining $\rho_{ivv'}$ and $U_{mm''m'''m'}$, the effective Hartree-Fock potential V^{HF} can then obtained.

In addition, orbital dependent J_m in H^{eff} can be straightforwardly obtained from the local site energy difference of Nd d -orbitals between spin-up and spin-down, when the $\frac{3}{2}$ -spin S_i^f of the f -orbitals are all set to be along the spin-up direction. Finally, the remaining intra-atomic hopping parameters $t_{iimm'}$ and site energy ε_m is then obtained by subtracting V^{HF} from the intra-atomic part of $H^{\text{LDA+}U}$.

A simple criterion to check the quality of the resulting H^{eff} (or the accuracy of the chosen U_{eff} and J_{eff}) is the degree of

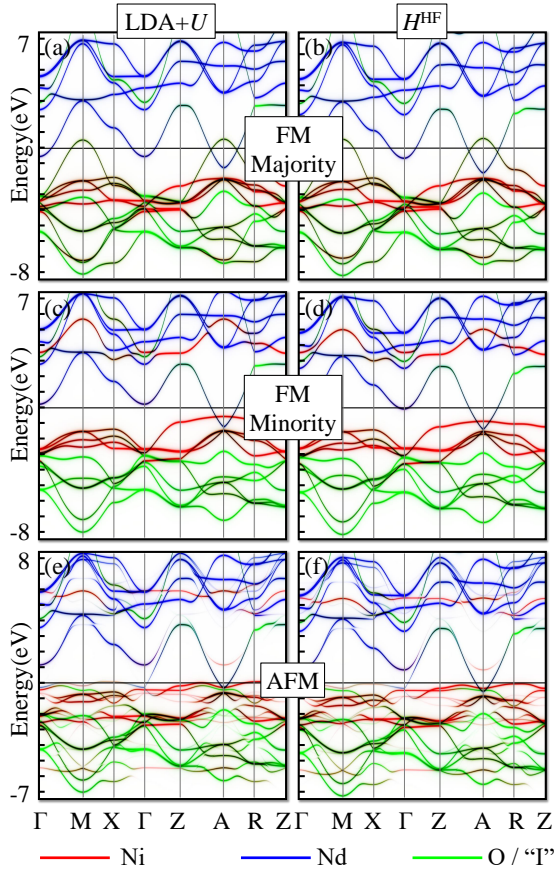


FIG. 4. Confirmation of the quality of H^{eff} by comparing the electronic band structures with those from LDA+U calculations under different magnetic configurations: (a)(b) spin majority of ferromagnetic order, (c)(d) spin minority of ferromagnetic order, and (e)(f) antiferromagnetic order. The excellent agreement establishes a robust foundation for configurations with non-collinear spin correlations without long-range order.

the spin-independence of the intra-atomic $t_{iimm'}$. A reasonable value of U_{eff} and J_{eff} should encode all the spin-dependence of the self-consistent H^{HF} . Therefore, a non-negligible spin-dependence of the resulting $t_{iimm'}$ or site energy ε_m indicates clearly a need to improve the value of U_{eff} and J_{eff} . In practice, we find this criterion quite sufficient to pin down a rather narrow range of acceptable values of U_{eff} and J_{eff} . This then allows us to fix all the intra-atomic parameters in H^{eff} .

On the other hand, since the LDA+U only included atomically local Hartree-Fock approximation, the inter-atomic hopping parameters $t_{iim'm'}$ are unaffected in the approximation. We therefore can simply take it from the spin-averaged $H^{\text{LDA+U}}$. The next section lists some of the leading parameters.

The above procedure, if performed properly, should generate a SU(2)-symmetric many-body Hamiltonian H^{eff} that can be further studied with any many-body solver one prefers, not just the Hartree-Fock approximation. Furthermore, since the Hamiltonian does not require or guarantee a magnetic order, it can in principle be applied to metallic systems (or spin liquid insulators) that do not contain long-range order but show

TABLE I. Leading parameters ε_m and J_m in unit of eV.

Nd	$d_{3z^2-r^2}$	$d_{x^2-y^2}$	d_{yz}	d_{xz}	d_{xy}
J_m	0.272	0.379	0.268	0.268	0.217
ε_m	4.12	5.43	5.779	5.779	4.045
Ni	$d_{3z^2-r^2}$	$d_{x^2-y^2}$	d_{yz}	d_{xz}	d_{xy}
ε_m	-55.448	-55.101	-55.616	-55.616	-55.284
O	p_x	p_y	p_z	"T"	
ε_m	-3.488	-2.542	-2.602	4.93	

signs of the existence of local moments, for example Curie-Weiss susceptibility at high-temperature.

For the purpose of this work, in which we study the impact of non-collinear spin correlations, we verify that H^{eff} is able to reproduce the $H^{\text{LDA+U}}$ solution under various magnetic orders. Figure 4 demonstrates an excellent correspondence between our resulting band structure under the same Hartree-Fock treatment of local interactions and the LDA+U band structure within the subspace of the selected orbitals. Notice especially that the agreement occurs under both ferromagnetic and antiferromagnetic order with the *same* set of parameters, despite the significantly different band structure under these two orders. These results thus establish the high quality of these parameters and the validity of our effective Hamiltonian in describing various magnetic structures, including the paramagnetic parent compound.

3. Leading parameters for H^{eff}

Table I lists some of the leading coefficients ε_m and J_m of the resulting SU(2) symmetric many-body Hamiltonian. The full interaction kernel $U_{mm'm'm'}$ is approximated by the Slater integral [31, 51], with $U_{\text{eff}} = 7.385$ eV and $J_{\text{eff}} = 1.197$ eV obtained from the above procedure. The leading terms of the resulting hopping parameters $t_{iim'm'}$ are 1.321 eV between Ni $d_{x^2-y^2}$ and O p_x , 1.158 eV between Nd d_{xz}/d_{yz} and O p_z , and 1.024 eV between Nd d_{xy} and "T" orbitals. The full $t_{iim'm'}$ parameters are available upon request.

4. Implementation of non-collinear magnetic configuration

In this study, the fluctuation of non-collinear spin directions is incorporated in our simulation by averaging large number of configurations with similar nearest short-range correlations $\chi = \sum_{\langle i, i' \rangle} \mathbf{S}_i \cdot \mathbf{S}_{i'}$, but with negligible long-range order $\mathbf{M}_q = \sum_i \mathbf{S}_i e^{i\mathbf{q} \cdot \mathbf{x}_i}$. Obviously, a larger supercell is necessary in the search for configurations of various short-range correlation, but without long-range order. Furthermore, averaging over large supercells with various sizes, shapes and orientations is an efficient way to avoid fictitious gap openings and shadow band foldings related to the artificial new spatial periodicity.

The enforcement of the spin directions according to the proposed magnetic configurations can be easily achieved within

the Hartree-Fock approximation by constraining the atomically local one-body density matrix $\rho_{ivv'}$ to be diagonal in the spin channel $v = v'$ along the assigned spin direction. Specifically, using the Euler angle we represent (rotate) $\rho_{ivv'}$ in a local spin basis whose z -axis is along the assigned spin direction. We then zero out the off-diagonal elements of $\rho_{ivv'}$ in this local basis, and then rotate the representation back to the global one with z -axis of the spin along that of the lattice. This constrained $\rho_{ivv'}$ is then combined with $U_{mm''m'''m'}$ in Eq.(1) to evaluate the effective orbital-dependent potential within the Hartree-Fock approximation. Naturally, the same constraint needs to be applied in each iteration of the self-consistent cycle, until a spin-density is converged.

* corresponding email: weiku@sjtu.edu.cn

[1] N. F. Mott, *Proceedings of the Physical Society. Section A* **62**, 416 (1949).

[2] N. F. Mott, *Rev. Mod. Phys.* **40**, 677 (1968).

[3] G.H.Jonker and J.H.Van Santen, *Physica* **16**, 337 (1950).

[4] F. Steglich, J. Aarts, C. D. Bredl, W. Lieke, D. Meschede, W. Franz, and H. Schäfer, *Phys. Rev. Lett.* **43**, 1892 (1979).

[5] M. R. Norman, *Science* **332**, 196 (2011).

[6] C. M. Varma, P. B. Littlewood, S. Schmitt-Rink, E. Abrahams, and A. E. Ruckenstein, *Phys. Rev. Lett.* **63**, 1996 (1989).

[7] Z. Fisk and G. W. Webb, *Phys. Rev. Lett.* **36**, 1084 (1976).

[8] P. Anderson, *Materials Research Bulletin* **8**, 153 (1973).

[9] E. Dagotto, *Rev. Mod. Phys.* **66**, 763 (1994).

[10] E. Dagotto, *Science* **309**, 257 (2005).

[11] L. Taillefer, *Annual Review of Condensed Matter Physics* **1**, 51 (2010).

[12] J. Zhao, Q. Huang, C. Cruz, S. Li, J. Lynn, Y. Chen, M. Green, G. Chen, G. Li, Z. Li, J. Luo, N. Wang, and P. Dai, *Nature Materials* **7**, 953 (2008).

[13] P. Schiffer, A. P. Ramirez, W. Bao, and S.-W. Cheong, *Phys. Rev. Lett.* **75**, 3336 (1995).

[14] M. Imada, A. Fujimori, and Y. Tokura, *Rev. Mod. Phys.* **70**, 1039 (1998).

[15] S. Nakatsuji and Y. Maeno, *Phys. Rev. Lett.* **84**, 2666 (2000).

[16] M. L. Foo, Y. Wang, S. Watauchi, H. W. Zandbergen, T. He, R. J. Cava, and N. P. Ong, *Phys. Rev. Lett.* **92**, 247001 (2004).

[17] Y. Cao, V. Fatemi, S. Fang, K. Watanabe, T. Taniguchi, E. Kaxiras, and P. Jarillo-Herrero, *Nature* **556**, 43 (2018).

[18] Y. Cao, V. Fatemi, A. Demir, S. Fang, S. L. Tomarken, J. Y. Luo, J. D. Sanchez-Yamagishi, K. Watanabe, T. Taniguchi, E. Kaxiras, and et al., *Nature* **556**, 80 (2018).

[19] M. Kawai, F. Nabeshima, and A. Maeda, *Journal of Physics: Conference Series* **1054**, 012023 (2018).

[20] D. Li, K. Lee, B. Y. Wang, M. Osada, S. Crossley, H. R. Lee, Y. Cui, Y. Hikita, and H. Y. Hwang, *Nature* **572**, 624 (2019).

[21] Y. S. Kushnirenko, A. A. Kordyuk, A. V. Fedorov, E. Haubold, T. Wolf, B. Büchner, and S. V. Borisenko, *Phys. Rev. B* **96**, 100504(R) (2017).

[22] D. Kang, Y. Zhou, W. Yi, C. Yang, J. Guo, Y. Shi, S. Zhang, Z. Wang, C. Zhang, S. Jiang, and et al., *Nature Communications* **6** (2015).

[23] X. Pan, Y. Pan, J. Jiang, H. Zuo, H. Liu, X. Chen, Z. Wei, S. Zhang, Z. Wang, X. Wan, Z. Yang, D. Feng, Z. Xia, L. Li, F. Song, B. Wang, Y. heng Zhang, and G. Wang, *Frontiers of Physics* **12**, 127203 (2017).

[24] J. Maletz, V. B. Zabolotnyy, D. V. Evtushinsky, S. Thirupathaiah, A. U. B. Wolter, L. Harnagea, A. N. Yaresko, A. N. Vasiliev, D. A. Chareev, A. E. Böhmer, F. Hardy, T. Wolf, C. Meingast, E. D. L. Rienks, B. Büchner, and S. V. Borisenko, *Phys. Rev. B* **89**, 220506(R) (2014).

[25] A. Fedorov, A. Yaresko, T. K. Kim, Y. Kushnirenko, E. Haubold, T. Wolf, M. Hoesch, A. Grueneis, B. Büchner, and S. V. Borisenko, *Sci Rep* **6** (2016).

[26] J. Nayak, K. Filsinger, G. H. Fecher, S. Chadov, J. Minár, E. D. L. Rienks, B. Büchner, S. P. Parkin, J. Fink, and C. Felser, *Proceedings of the National Academy of Sciences* **114**, 12425 (2017).

[27] I. A. Nekrasov, N. S. Pavlov, and M. V. Sadovskii, *Journal of Experimental and Theoretical Physics* **126** (2018).

[28] P. Hohenberg and W. Kohn, *Phys. Rev.* **136**, B864 (1964).

[29] W. Kohn and L. J. Sham, *Phys. Rev.* **140**, A1133 (1965).

[30] V. I. Anisimov, I. V. Solovyev, M. A. Korotin, M. T. Czyżk, and G. A. Sawatzky, *Phys. Rev. B* **48**, 16929 (1993).

[31] A. I. Liechtenstein, V. I. Anisimov, and J. Zaanen, *Phys. Rev. B* **52**, R5467 (1995).

[32] See supplementary Material for the calculation details, leading parameters, discussions on the many-body Hamiltonian.

[33] A. D. Becke, *The Journal of Chemical Physics* **98**, 1372 (1993).

[34] W. Ku, H. Rosner, W. E. Pickett, and R. T. Scalettar, *Phys. Rev. Lett.* **89**, 167204 (2002).

[35] W.-G. Yin, D. Volja, and W. Ku, *Phys. Rev. Lett.* **96**, 116405 (2006).

[36] N. Marzari and D. Vanderbilt, *Phys. Rev. B* **56**, 12847 (1997).

[37] K. S. Thygesen, L. B. Hansen, and K. W. Jacobsen, *Phys. Rev. B* **72**, 125119 (2005).

[38] F. Gygi, J.-L. Fattebert, and E. Schwegler, *Computer Physics Communications* **155**, 1 (2003).

[39] F. Giustino and A. Pasquarello, *Phys. Rev. Lett.* **96**, 216403 (2006).

[40] Y. Nomura, M. Hirayama, T. Tadano, Y. Yoshimoto, K. Nakamura, and R. Arita, *Physical Review B* **100**, 205138 (2019).

[41] W. Ku, T. Berlijn, and C.-C. Lee, *Physical Review Letters* **104**, 216401 (2010).

[42] Y.-T. Tam, D.-X. Yao, and W. Ku, *Phys. Rev. Lett.* **115**, 117001 (2015).

[43] Z.-J. Lang, R. Jiang, and W. Ku, *Phys. Rev. B* **103**, L180502 (2021).

[44] Z.-J. Lang, R. Jiang, and W. Ku, *Phys. Rev. B* **105**, L100501 (2022).

[45] N. Ghosh, A. Bharathi, A. Satya, S. Sharma, A. Mani, R. Sarguna, D. Sornadurai, V. Sastry, and C. Sundar, *Solid State Communications* **150**, 1940 (2010).

[46] X. Ren, W.-C. Chen, J. Li, Q. Gao, J. J. Sanchez, H. Luo, F. Rodolakis, J. L. McChesney, J. W. Freeland, T. Xiang, J.-H. Hu, R. Comin, Y. Wang, X. Zhou, and Z. Zhu, (2021), 2109.05761.

[47] K. Iida, J. Hänsch, R. Hühne, F. Kurth, M. Kidszun, S. Haindl, J. Werner, L. Schultz, and B. Holzapfel, *Applied Physics Letters* **95**, 192501 (2009).

[48] D. J. Singh, *Planewaves, Pseudopotentials and the LAPW Method* (Springer New York, NY, New York, 2006).

[49] P. Blaha, K. Schwarz, P. Sorantin, and S. Trickey, *Computer Physics Communications* **59**, 399 (1990).

[50] V. I. Anisimov, F. Aryasetiawan, and A. I. Lichtenstein, *Journal of Physics: Condensed Matter* **9**, 767 (1997).

[51] J. Slater, *Quantum Theory of Molecules and Solids* (Mcgraw-Hill, New York, 1974).